Superconductivity in the ternary antimonide La_6ZnSb_{15}

Makoto Wakeshima, Chiho Sakai, and Yukio Hinatsu

Division of Chemistry, Graduate School of Science, Hokkaido University

Sapporo 060-0810, Japan

Abstract

We discovered superconductivity in the ternary antimonide La_6ZnSb_{15}, and its superconducting properties were discussed through the resistivity, specific heat, and magnetization measurements. The crystal structure of La_6ZnSb_{15} is the orthorhombic La_6MnSb_{15}-type structure consisting of Sb sheets. Its electronic structure indicates that the conduction bands are mainly originated from Sb 5*p* orbitals in these Sb sheets. The electrical resistivity and magnetization measurements reveal that this compound is a type-II superconductor below 3.7 K. The upper critical field at zero temperature, $\mu_0 H_{c2}(0)$, is determined to be 851(8) mT. In the normal state, the electronic specific heat coefficient, γ, and the Debye temperature, Θ_D, are found to be 18.8(8) mJ/mol K^2 and 218(1) K, respectively. From the electronic specific heat in the superconducting state, this compound belongs to a typical weak-coupling BCS superconductor.

Introduction

Late main group elements (Si, Ge, Sn, Pb, P, As, Sb, Bi, Se, Te) frequently built diverse and important intermetallic mosaics. In particular, antimony shows attractive structural and bonding characteristics, i.e. Sb-Sb bondings form in infinite networks such as one-dimensional chain and two-dimensional square sheet [1,2]. Recently, Papoian and Hoffman discussed the infinite networks consisting of the Sb-Sb bondings for some binary and ternary antimonides by using the analogy between the Zintl concept and the octet rule [2].

Such infinite networks consisting of Sb-Sb bondings are also found in the $Ln_6M\mathrm{Sb}_{15}$ (*Ln* = lanthanides, *M* = Mn, Cu, Zn) compounds which were synthesized by Cordier and co-workers [3-5]. These compounds crystallize in the $\mathrm{La}_6\mathrm{MnSb}_{15}$-type orthorhombic structure (space group *Imm*2 ; *a* ~15 Å, *b* ~ 19 Å, *a* ~ 0.4 Å ; *Z* = 2). Figure 1 shows the schematic crystal structure of $Ln_6M\mathrm{Sb}_{15}$. In this structure, antimony atoms make up two-dimensional sheets and transition metals connect the antimony sheets. Transition metals randomly occupy ~50 % of the 4*c* site. One-dimensional $Ln_3\mathrm{Sb}$ chains along the *c* axis are located in this three-dimensional Sb network. For their magnetic properties, $\mathrm{Ce}_6\mathrm{MnSb}_{15}$ and $\mathrm{Gd}_6\mathrm{ZnSb}_{15}$ show an antiferromagnetic transition [5]. For $\mathrm{La}_6\mathrm{MnSb}_{15}$, the bonds were investigated in detail through a molecular orbital analysis by Papoian and Hoffman [6]. They pointed out that significant La-Sb network interactions exist. These $Ln_6M\mathrm{Sb}_{15}$ compounds are expected to show interesting physical properties due to the Sb network and the one-dimensional $Ln_3\mathrm{Sb}$ chains.

Thus, we have investigated the transport and magnetic properties of the $Ln_6\mathrm{ZnSb}_{15}$ compounds. In this paper, the superconductivity of $\mathrm{La}_6\mathrm{ZnSb}_{15}$ is reported through studies of the electrical resistivity, magnetic susceptibility, magnetization, and specific heat studies.

Experimental

Samples were prepared from stoichiometric mixtures of the elements: La powder (99.9 %), Zn powder (99.99 %), and Sb powder (99.99 %). The mixture was pressed into a pellet and then sealed in an evacuated quartz tube. The sample was preheated at 600 °C for 3 h. The reaction was carried out at 600 ~ 900 °C for ~100 h, with regrinding at several intervals.

Powder X-ray diffraction measurement was carried out in the region of $10° \leq 2\theta \leq 120°$ at intervals of 0.02° using Cu $K\alpha$ radiation on a Rigaku MultiFlex diffractometer equipped with a curved graphite monochromator. The crystal structure was determined by the Rietveld technique, using the program RIETAN 2000 [7].

The calculation of the electronic structure and the density of states (DOS) are studies using the WIEN2k program [8] using the full potential linearized augmented plane wave+local orbitals (FP-LAPW+lo) method based on the density functional theory (DFT) with the generalized gradient approximation (GGA).

The temperature dependence of the magnetic susceptibilities was measured under both zero-field-cooled condition (ZFC) and field-cooled condition (FC) in the temperature range between 1.8 K and 300 K by using the SQUID magnetometer (Quantum Design, MPMS-5S). The magnetic field dependence of the magnetization was measured at 1.8 K by changing the applied magnetic field between −500 and 500 mT. The volume fraction of the superconducting phase was estimated from the FC magnetization in a field of 1 mT.

Electrical resistivity measurements were carried out in the temperature range 0.4 ~ 400 K and in magnetic fields up to 800 mT by the standard four-probe method in a Quantum Design Physical Property Measurement System (PPMS) equipped with a ^{3}He refrigerator. The applied current was 500 μA. The sintered sample was cut into a piece

having sizes of approximately 2.5 × 0.3 × 5 mm^3. Four Au wires were painted onto the samples using silver paste.

Specific heat measurements were performed by the thermal relaxation in the temperature range between 0.4 K and 300 K with the PPMS. The sintered sample (~15 mg) was mounted on a thin alumina plate with Apiezon N grease for better thermal contact.

Results and discussion

Crystal and electronic structures

The La_6ZnSb_{15} phase was identified from the X-ray diffraction (XRD) profile. The profile is indexed with an orthorhombic La_6MnSb_{15}-type cell with space group *Imm*2. From the Rietveld refinement, the calculated diffraction profile agrees well with the observed one as shown in Fig. 2, and the reliability factors are found to be 12.2 % for R_{wp} and 6.5 % for R_I. The atomic displacement parameters are fixed to be the reported value [5]. The lattice parameters *a*, *b*, and *c* were obtained to be 15.370(3) Å, 19.420(4) Å, and 4.361(1) Å, respectively, and these values and the positional parameters are in good agreement with the reported ones [5].

Figure 3 shows the total DOS and individual DOS of Zn for $La_6Zn_xSb_{15}$ (x = 0, 2). These features of the band structures are similar to that of La_6MnSb_{15} [6]. In the present compound, zinc atoms occupy randomly 50 % of the 4*c* site. The DOS calculation have been performed on the assumption that zinc atoms occupy the 4*c* site without deficiency, i.e. "$La_6Zn_2Sb_{15}$" is used for the band structure calculation as a "formal" chemical formula. The calculation reveals that the energy level (~7.8 eV) of the band (the band width ~1 eV) consisting of Zn *d* orbitals is much lower than the Fermi level and that the hybridization of Zn orbitals with valence band states is almost negligible near the Fermi level. The total DOS at the Fermi level, $N(E_F)$, is obtained to be 7.37 states / eV f.u. (f.u. : formula unit). In

order to check the effect of Zn deficiencies on the band structure, we have computed the band structure of "$La_6Zn_0Sb_{15}$" with exception of Zn, also. The Fermi level shifts toward lower energy (~0.5 eV). The total $N(E_F)$ is determined to be 6.53 states / eV f.u. and this value is 10 % lower than that for "$La_6Zn_2Sb_{15}$". We assume that the value of $N(E_F)$ for "La_6ZnSb_{15}" is ~7 states / eV f.u.. The calculations for both of "$La_6Zn_2Sb_{15}$" and "$La_6Zn_0Sb_{15}$" also reveal that the conduction bands around the Fermi level mainly consist of the Sb1, Sb2, and Sb5 atoms in the two-dimensional Sb sheets and secondarily consist of La1 and La2 atoms in the one-dimensional La_3Sb chains.

Electrical resistivity

Figure 4 (a) shows the temperature dependence of the electrical resistivity for La_6ZnSb_{15}. Above 4 K, this compound exhibits a typical metallic behavior up to 400 K, but with some negative curvature for $\rho(T)$ with increasing temperature. Based on the Matthiensen's rule, the resistivity for nonmagnetic metallic compounds is represented by the Bloch-Grüneisen (BG) model for Debye phonons [9].

$$\rho(T) = \rho_0 + \rho_{ph} + \rho_{e\text{-}e}$$

$$= \rho_0 + 4Nk_B\Theta_D\left(\frac{T}{\Theta_D}\right)^5 \int_0^{\Theta_D/T} \frac{x^5 dx}{\left(e^x - 1\right)\left(1 - e^{-x}\right)} + \rho_{e-e}, \qquad (1)$$

where k_B and Θ_D are the Boltzman constant and the Debye temperature, respectively. Third term expresses the resistivity by electron-electron interaction. The Debye temperature is about 200 K as will be described later, but the model with Θ_D = 200 K fails to fit to the observed ρ data at low temperatures, i.e. a rapid rise of ρ with increasing temperature below 30 K could not be explained from a change in the resistivity by phonon scatterings. The ρ-T^2 curve is plotted in the inset of Fig. 4 (a). The ρ is proportional to be T^2 below 30

K, which indicates that the effect of electron-electron interaction ($\rho_{e\text{-}e}$) predominates for a change in the resistivity at low temperatures [10].

Figure 4 (b) shows the temperature dependence of the electrical resistivity below 5 K in various magnetic fields for La_6ZnSb_{15}. Below 3.85 K, the resistivity in the zero-field drops sharply, indicating a phase transition to a superconducting state. The onset temperature is 3.85 K and zero resistivity is attained below 3.65 K. The critical temperature T_c is defined as the midpoint of the transition; $T_c^{mid,R}$ = 3.74 K. The electronic structure calculation suggests that the two-dimensional Sb sheets and the one-dimensional La_3Sb chains raise this superconducting state.

With increasing magnetic field, T_c decrease monotonously. Assuming that this compound is a type-II superconductor, as will be justified below, the upper critical fields, $\mu_0 H_{c2}(T)$, were estimated from the critical temperature T_c^R which is determined as an intersection of the extrapolated normal-state resistivity and the steep part of $\rho(H, T)$ at several applied fields. Figure 5 shows $\mu_0 H_{c2}(T)$ as a function of critical temperature. The Werthamer–Helfand–Hohenberg (WHH) theory for a type-II superconductor predicts that $\mu_0 H_{c2}(T)$ is proportional to $(1 - T/T_c)$ near T_c, in either the "clean" or the "dirty" limit [11]. However, the $\mu_0 H_{c2}(T)$-T curve reveals that $\mu_0 H_{c2}(T)$ does not intersect the T axis linearly but bends towards the higher T side giving $d^2\mu_0 H_{c2}(T) / dT^2 > 0$. For a large number of superconductors, a similar positive curvature in $\mu_0 H_{c2}(T)|_{T \to T_c}$ has been observed [12-16].

The positive curvature in $\mu_0 H_{c2}(T)|_{T \to T_c}$ makes it difficult to apply the WHH theory. Thus, in order to obtain $[d\mu_0 H_{c2} / dT]_{T=T_c}$, the $\mu_0 H_{c2}$ data in the temperature range of 0.7 $T_c < T <$ 0.9 T_c is fitted to a straight line (a solid line in Fig. 3). The goodness of the fit is measured by the square of the correlation coefficient ($r^2 > 0.9995$). According

to the WHH theory in a dirty limit, the upper critical field at zero temperature can be estimated by using the following relation [11],

$$\mu_0 H_{c2}(0) = 0.693\, T_c \left(-\frac{d\mu_0 H_{c2}}{dT} \right)_{T \sim T_c} . \quad (2)$$

From the estimated $[d\mu_0 H_{c2} / dT]_{T=T_c}$ in the liner region, the $\mu_0 H_{c2}(0)$ value is derived to be 756(4) mT. However, the $\mu_0 H_{c2}$ value (~ 800 mT) near 0.5 K already exceeds this $\mu_0 H_{c2}(0)$ value. Therefore, in order to estimate the actual $\mu_0 H_{c2}$ value at zero temperature, we fitted the polynomial function to the observed $\mu_0 H_{c2}(T)$-T data below 2 K and the extrapolation to zero temperature leads that $\mu_0 H_{c2}(0)$ is 810(6) mT (see Fig. 5). Hereafter, we will adopt this value (= 810 mT) as $\mu_0 H_{c2}(0)$. The value of Ginzburg-Landau (GL) coherence length at zero temperature $\xi_{GL}(0)$ can be estimated to be 201 Å by the following equation,

$$\mu_0 H_{c2}(0) = \frac{\Phi_0}{2\pi \xi_{GL}(0)^2} , \quad (3)$$

where Φ_0 is the magnetic flux quantum.

Magnetic susceptibility and magnetization

Figure 6 (a) shows the temperature dependence of the ZFC and FC magnetic susceptibility χ. The magnetic susceptibility abruptly drops below 3.8 K, indicating a superconducting phase transition. The Meissner volume fraction is estimated to be 19.2 % from the FC susceptibility at 1.8 K. Figure 6 (b) and the inset of Fig. 6 (c) represent the magnetization versus magnetic field (M-H) curve at 1.8 K in the magnetic field ranges of -500 mT $\le H \le$ 500 mT and 0 mT $\le H \le$ 5 mT, respectively. These M-H curves indicate a typical type-II superconductor. As shown in the inset of Fig. 6 (c), the M-H curve indicates the linear dependence of the magnetization on field cause by Meissner effect at low fields.

The difference (ΔM) between this linear "Meissner" line and the observed data is plotted in Fig. 6 (c) and the lower critical field $\mu_0 H_{c1}$ at 1.8 K is found to be ~ 1 mT. The lower critical field $\mu_0 H_{c1}(0)$ at the zero temperature will be discussed later.

Specific heat

The temperature dependence of the specific heat (C) divided by temperature for La_6ZnSb_{15} is shown in Fig. 7 (a). A jump in the specific heat is observed starting at 3.85 K indicative of the bulk superconducting transition. The critical temperature from specific heat data is defined as the midpoint of the transition; $T_c^{\mathrm{mid},C}$= 3.61 K. We assume that the total specific heat is composed of the electron and phonon contributions, $C(T) = C_e(T) + C_{ph}(T)$. In the normal state, the phonon contribution is expressed by the βT^3 term at the temperature much below the Debye temperature Θ_D, and the electronic specific heat C_{en} is proportional to be temperature.

$$C(T)/T = \beta T^2 + \gamma = \frac{12 n \pi^4 R}{5 \Theta_D{}^3} T^2 + \gamma . \qquad (4)$$

From the $C(T)/T$ vs T^2 plot, Θ_D and the electronic specific heat coefficient γ values were obtained to be 214.5(8) K and 18.8(7) mJ/mol K^2, respectively. The electron-phonon coupling constant $\lambda_{e\text{-}ph}$ which appears in the McMillan equation for the superconducting transition temperature T_c. The value of λ is estimated form the McMillan equation [17],

$$k_B T_c = \frac{\hbar \omega_{\log}}{1.2} \exp\left[-\frac{1.04(1+\lambda_{e\text{-}ph})}{\lambda_{e\text{-}ph} - \mu^*(1+0.62\lambda_{e\text{-}ph})} \right] \qquad (5)$$

where k_B is Boltzmann constant and $\omega_{\log}$ is taken to be 0.7 ω_{ph}, ω_{ph} is regarded to be the same as the Debye frequency $\omega_D = k_B \Theta_D / \hbar$, and μ^* is Coulomb pseudopotential and is usually taken between 0.1 and 0.15. The value of $\lambda_{e\text{-}ph}$ is determined to be 0.61 for μ^* = 0.1

and 0.72 for μ^* = 0.15. This small $\lambda_{e\text{-}ph}$ value suggests that La_6ZnSb_{15} is classified into weak-coupling superconductors.

The electron-phonon coupling parameter can also be obtained from the ratio of

$$\frac{N_{obs}(E_F)}{N_{band}(E_F)} = \frac{\gamma_{obs}}{\gamma_{band}} = 1 + \lambda_\gamma , \quad (6)$$

where λ_γ is the electron-phonon mass enhancement parameter. which should be similar to $\lambda_{e\text{-}ph}$ [17]. The calculated value of γ_{band} ($=\frac{\pi^2}{3} N_A k_B{}^2 N(E_F)$) is 16.5 mJ/mol K^2 with $N(E_F)$ = ~7 states / eV f.u. and the value of λ_γ is derived to be 0.1 from γ_{obs} and γ_{band}. This small λ_γ is also indicative of a weak electron-phonon coupling. The discrepancy between $\lambda_{e\text{-}ph}$ and λ_γ is attributable to a rough estimation of DOS of La_6ZnSb_{15} at the Fermi level.

Figure 7 (b) exhibits the difference in the specific heat ($\delta C_{es}/T = (C_{es} - C_{en})/T$) between the superconducting state and the normal state. In the inset, the difference in the entropy change ($S = \int_0^{T_c} (\delta C_{es}/T) dT$) between the superconducting and normal states is plotted, indicating the entropy conservation which is essential for a second order superconducting-normal phase transition around the transition temperature. The specific heat jump ΔC at the $T_c^{mid,C}$ shows an evident energy gap under the superconducting state. As shown in Fig. 7 (b), the scaled specific heat jump values $\Delta C / \gamma T_c^{mid,C}$ are 1.46. This value is good agreement the theoretical value of 1.43 for a limit weak-coupling superconductor predicted from the BCS theory.

Figure 7 (c) displays the Arrhenius plot of the electronic specific heat. The temperature dependence of the electronic specific heat for after superconducting transition, C_{es}, reflects clearly an exponential behavior, indicating of a gap character like as shown in an *s*-wave superconductor. The solid line represents the best fitting result (C_{es} =

$8.14\gamma T_c\exp(-1.46T_c/T)$ J/mol K) in the temperature range of $2 < T_c/T < 5$. For a weak-coupled BCS superconductor, C_{es} follows the relations ; $C_{es} = 8.5\gamma T_c\exp(-1.44T_c/T)$ for $2.5 < T_c/T < 6$, $C_{es} = 26\gamma T_c\exp(-1.62T_c/T)$ for $7 < T_c/T < 12$, and $C_{es} = 3.15\gamma T_c(T_c/T)^{3/2}\exp(-1.76T_c/T)$ for $T \to 0$ [18]. On comparing these equations with the experimental curve, it is suggests that C_{es} of La_6ZnSb_{15} follows reasonably well the prediction of the BCS model.

The temperature dependence of the thermodynamical critical field $\mu_0 H_c$ is obtained by integrating the experimental data in the superconducting state using

$$\Delta G = \frac{1}{2}\mu_0 V_M {H_c}^2(T) = \int_T^{T_c}\int_{T'}^{T_c}\frac{C_{es}(T'') - \gamma T''}{T''}dT''dT' \qquad (7)$$

where V_M represents the volume per mole. Figure 7 (d) shows the temperature dependence of the thermodynamical critical field $\mu_0 H_c$. The zero temperature value $\mu_0 H_c(0)$ is obtained to be 16.9 mT. Substituting this value of $\mu_0 H_c(0)$ into

$$\mu_0 V {H_c}^2(0) = \left(\frac{3\gamma}{2\pi^2 {k_B}^2}\right)\Delta(0)^2 \qquad (8)$$

The superconducting energy gap at zero temperature, $\Delta(0)$ can be estimated to be 0.48 meV. Therefore, its scaled value of $2\Delta(0)/k_B T_c^{mid,C}$ is found to be 3.09, which is smaller than the isotropic BCS value of 3.53.

Moreover, the penetration depth $\lambda_{GL}(0)$, GL parameter $\kappa(0)$ and lower critical field at 0 K $\mu_0 H_{c1}(0)$ are estimated from the following relations,

$$\mu_0 H_c(0) = \frac{\Phi_0}{2\sqrt{2}\pi\lambda_{GL}(0)\xi_{GL}(0)}, \qquad (9)$$

$$\kappa(0) = \frac{\lambda_{GL}(0)}{\xi_{GL}(0)}, \qquad (10)$$

$$\mu_0 H_{c1}(0) = \frac{\mu_0 H_c(0)}{\sqrt{2}\kappa}\ln\kappa. \qquad (11)$$

The $\lambda_{GL}(0)$, $\kappa(0)$ and $\mu_0 H_{c1}(0)$ are estimated to be 6850 Å, 34.1 and 1.23 mT, respectively. This value of $\mu_0 H_{c1}(0)$ is consistent with the value obtained from the *M-H* curve (see Fig. 6 (c)). The value of $\kappa(0)$ suggest that La_6ZnSb_{15} is a typical type-II superconductor. These superconducting parameters are summarized in Table 1.

Summary

We found that a ternary antimonide La_6ZnSb_{15} consisting of two-dimensional Sb sheets and one-dimensional La chains is a superconductor with a critical temperature T_c, of about 3.7 K. The electronic structure calculation suggests that the Sb sheets raise the superconducting state. The $\mu_0 H_{c2}(0)$ values is estimated from T_c of electrical resistivity under the magnetic fields to be 810(6) mT. From specific heat measurements, γ, Θ_D, $\Delta C/\gamma T_c$ and $2\Delta/k_B T_c$ are 18.8(7) mJ/mol K^2, 214.5(8) K, 1.46 and 3.09 respectively. We conclude that this compound is a typical type-II superconductor with weak-coupling in the category of the BCS theory.

References

[1] Mills A M, Lam R, Ferguson M J, Deakin L and Mar A 2002 *Cood. Chem. Rev.* **233-234** 207

[2] Papoian G and Hoffmann R 2001 *J. Am. Chem. Soc.* **123** 6600

[3] Cordier G, Woll P and Schäfer H *paper P4A5, presented at the 8th Intl. Conference on Solid Compounds of Transition Elements* April 9–13, 1985

[4] Woll P 1985 *Thesis, Technical University, Darmstadt*

[5] Sologub O, Vybornov M, Rogl P, Hiebl K, Cordier G and Woll P 1996 *J. Solid State Chem.* **122** 266

[6] Papoian G and Hoffmann R 1998 *J. Solid State Chem.* **139** 8

[7] Izumi F and Ikeda T 2000 *Mater. Sci. Forum* **321-324** 198

[8] Blaha P, Schwarz K, Madsen G K H, Kvasnicka D and Luitz J 2001 *WIEN2k*, *An Augmented Plane Wave Plus Local Orbitals Program for Calculating Crystal Properties. ISBN 3-9501031- 1-2*, Vienna University of Technology, Austria

[9] Mott N F and Jones H 1958 *The Theory of the Properties of Metals and Alloys*, (Dover, New York)

[10] A. A. Abrikosov 1988 *Fundamentals of the Theory of Metals*, (North Holland, Amsterdam)

[11] Werthamer N R, Helfand E and Hohenberg P C 1966 *Phys. Rev.* **147** 295

[12] Prober D E, Schwall R E and Beasley M R 1980 *Phys. Rev. B* **21** 2717

[13] Coleman R V, Eiserman G K, Hillenius S J, Mitchell A T and Vicent J L 1983 *Phys. Rev. B* **27** 125

[14] Baenitz M, Heinze M, Lüders K, Werner H, Schlögl R, Weiden M, Sparn G and Steglich F 1995 *Solid State Commun.* **96** 539

[15] Mackenzie A P, Julian S R, Lonzarich G G, Carrington A, Hughes S D, Liu R S and Sinclair D S 1993 *Phys. Rev. Lett.* **71** 1238

[16] Rathnayaka K D D, Bhatnagar A K, Parasiris A, Naugle D G, Canfield P C and Cho B K 1997 *Phys. Rev. B* **55** 8506

[17] McMillan W L 1968 *Phys. Rev*. **167** 331

[18] Gopal E S R 1966 *Specific Heat at Low Temperatures* (Plenum, New York)

Figure Captions

Figure 1. Schematic crystal structure of La_6ZnSb_{15}.

Figure 2. X-ray diffraction profile for La_6ZnSb_{15}. The calculated and observed diffraction profiles are shown on the top solid line and cross markers, respectively. The vertical marks in the middle show positions calculated for Bragg reflections. The bottom trace is a plot of the difference between calculated and observed intensities.

Figure 3. Total and individual density of states (DOS) of $La_6Zn_xSb_{15}$ (x = 0, 2). The gray area shows the DOS of Zn.

Figure 4. (a) Temperature dependence of the electrical resistivity (ρ) below 400 K for La_6ZnSb_{15}. The inset shows the ρ-T^2 plot. (b) Temperature dependence of ρ below 5 K under various magnetic fields.

Figure 5. Temperature dependence of the upper critical fields ($\mu_0 H_{c2}$) for La_6ZnSb_{15} determined from the electrical resistivity data. The dotted line represents the extrapolation to zero temperature by the polynomial function.

Figure 6. (a) Temperature dependence of the magnetic susceptibility (χ) for La_6ZnSb_{15}. (b) Magnetization (M) as a function of the magnetic field at 1.8 K. (c) Magnetic field dependence of difference (ΔM) between the linear "Meissner" line and the observed data. The inset shows the M-H plot (open circle) at low fields and the "Meissner" line (solid line).

Figure 7. (a) Temperature dependence of specific heat (C_p/T) divided be temperature of La_6ZnSb_{15}. (b) Temperature dependence of the difference ($\delta C_{es}/T = (C_{es} - C_{en})/T$) in the specific heat divided by temperature between the superconducting state and the normal state. In the inset, the difference in the entropy change

between the superconducting and normal states is plotted, indicating the entropy conservation around the transition temperature. (c) Logarithmic C_{es} vs T_c/T in the superconducting state. The solid line is the linear fit to the data for T_c/T between 2 and 5. (d) Temperature dependence of the thermodynamical critical fields ($\mu_0 H_c$) determined from the specific heat data.

Table 1 Superconducting and normal-state properties for La_6ZnSb_{15}

V_M / m^3 mol^{-1}	3.92×10^{-4}
$T_c^{mid,R}$ / K	3.74
$T_c^{mid,C}$ / K	3.61
γ / mJ $mol^{-1}\cdot K^{-2}$	18.8
Θ_D / K	214
$\Delta C/\gamma T_c^{mid,C}$	1.46
$2\Delta(0)/k_B T_c^{mid,C}$	3.09
$\mu_0 H_{c2}(0)$ / mT	810
$\mu_0 H_c(0)$ / mT	16.9
$\mu_0 H_{c1}(0)$ (mT)	1.23
$\xi_{GL}(0)$ / Å	201
$\lambda_{GL}(0)$ / Å	6850
$\kappa(0)$	34.1

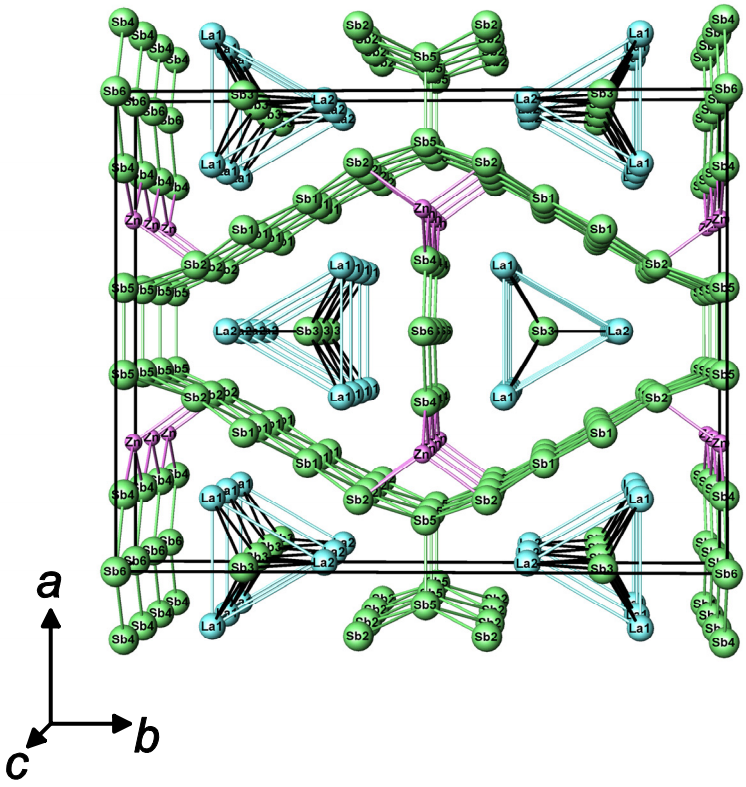

Fig.1

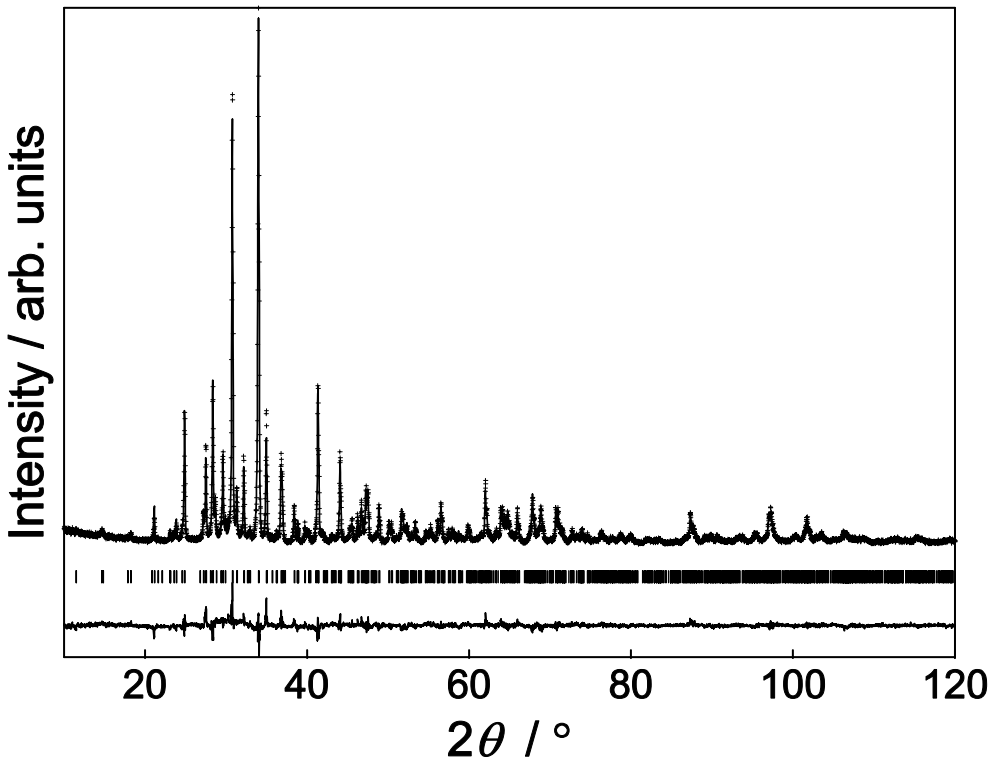

Fig.2

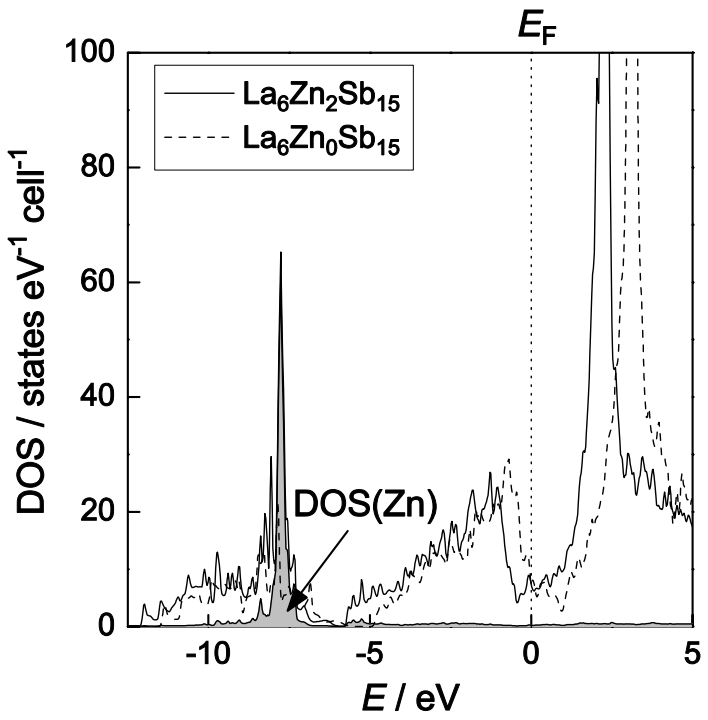
E_F
100
80
60
40
20
0
DOS / states eV^{-1} cell^{-1}
$La_6Zn_2Sb_{15}$
$La_6Zn_0Sb_{15}$
DOS(Zn)
-10
-5
0
5
E / eV

Fig.3

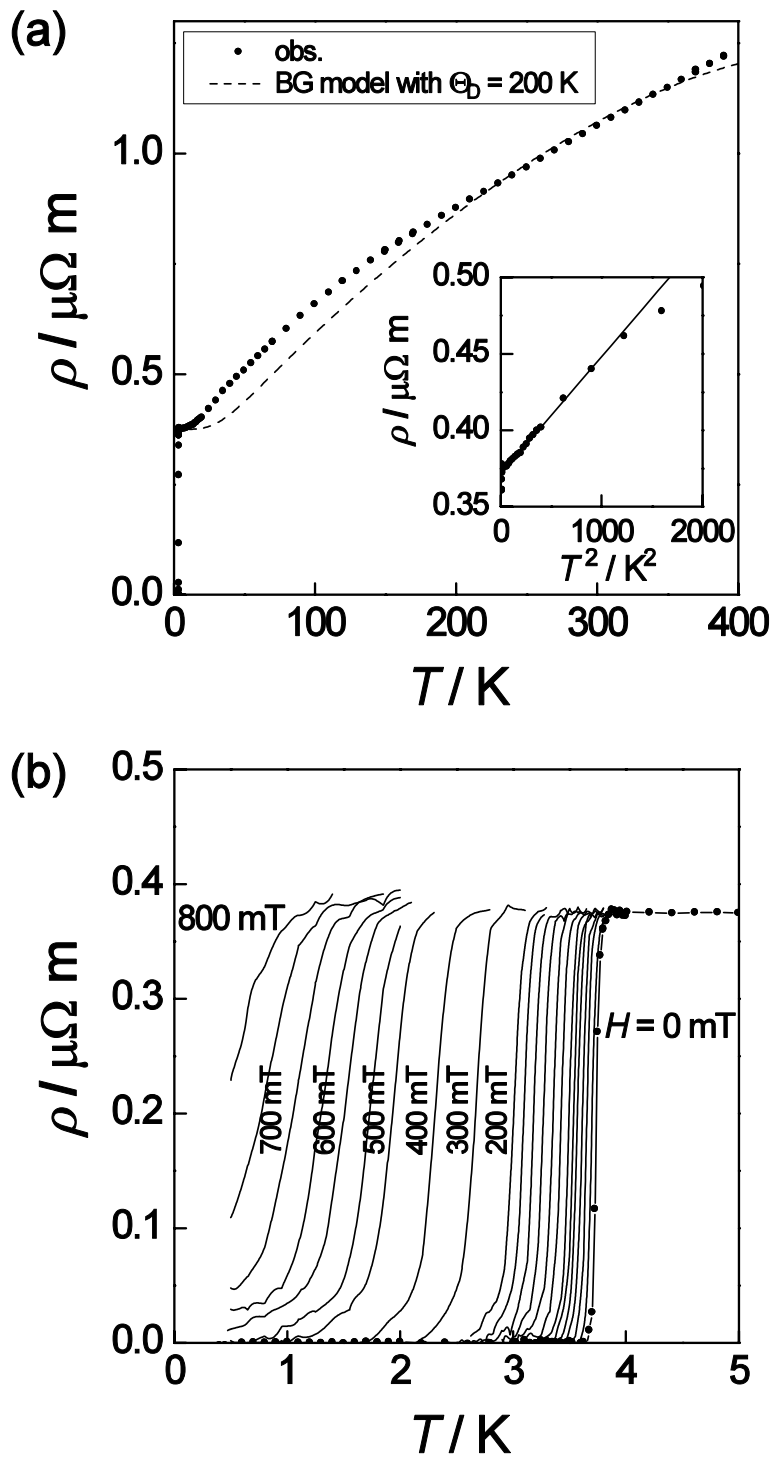
(a)
obs.
BG model with Θ_D = 200 K
ρ / μΩ m
T / K
T^2 / K^2
(b)
800 mT
700 mT
600 mT
500 mT
400 mT
300 mT
200 mT
H = 0 mT

Fig.4

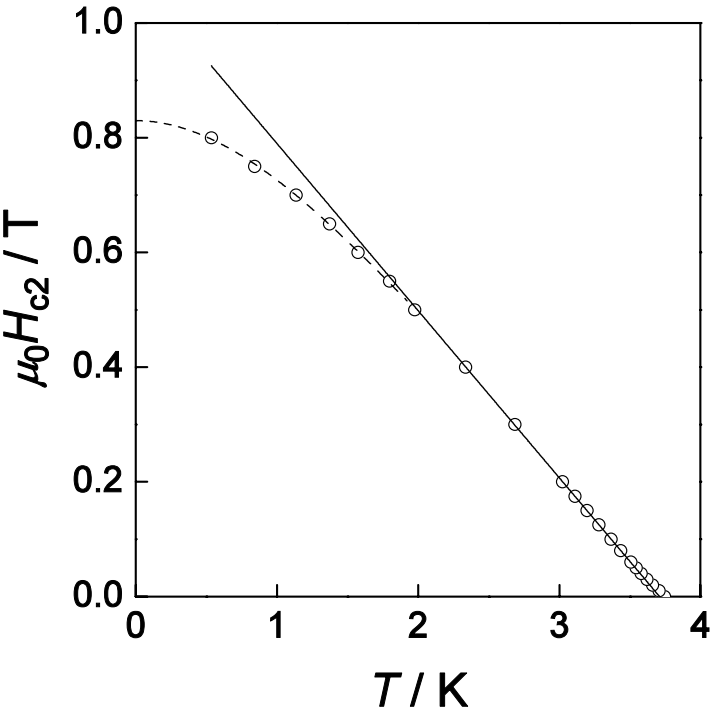

Fig.5

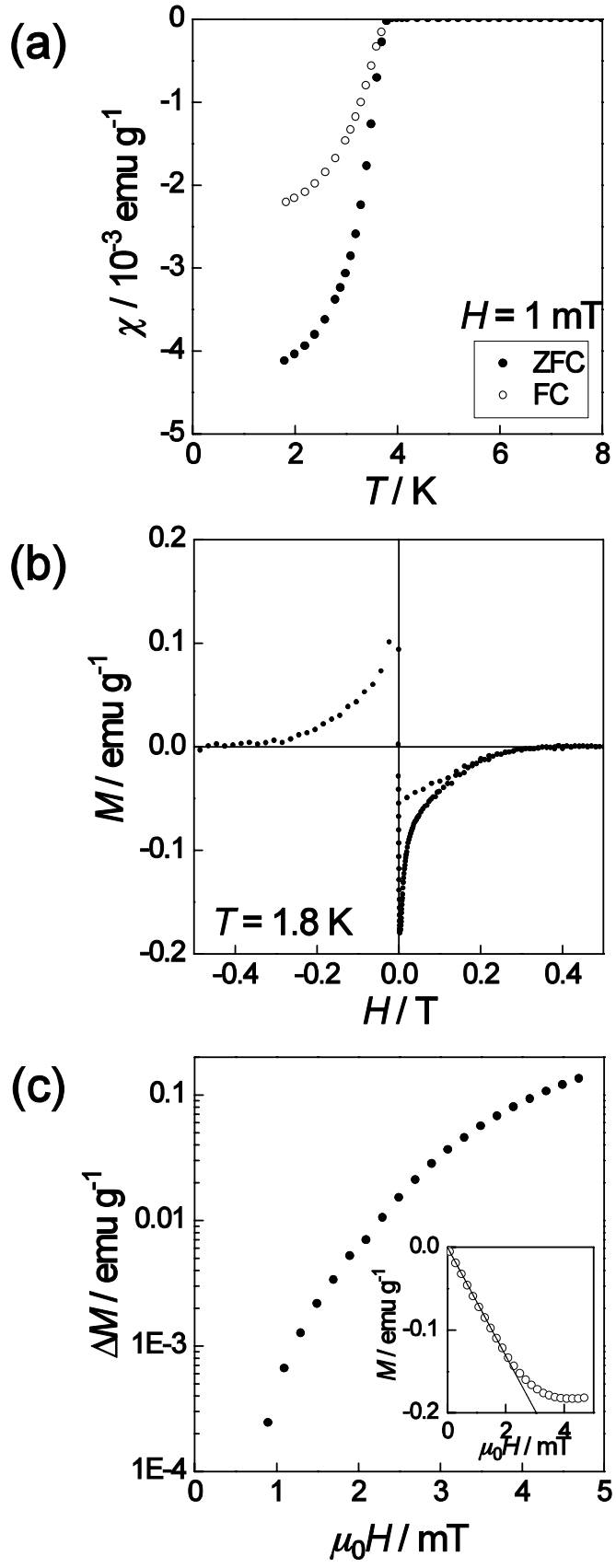
(a)
χ / 10-3 emu g-1
H = 1 mT
ZFC
FC
T / K
(b)
M / emu g-1
T = 1.8 K
H / T
(c)
ΔM / emu g-1
M / emu g-1
μ0H / mT
μ0H / mT

Fig.6

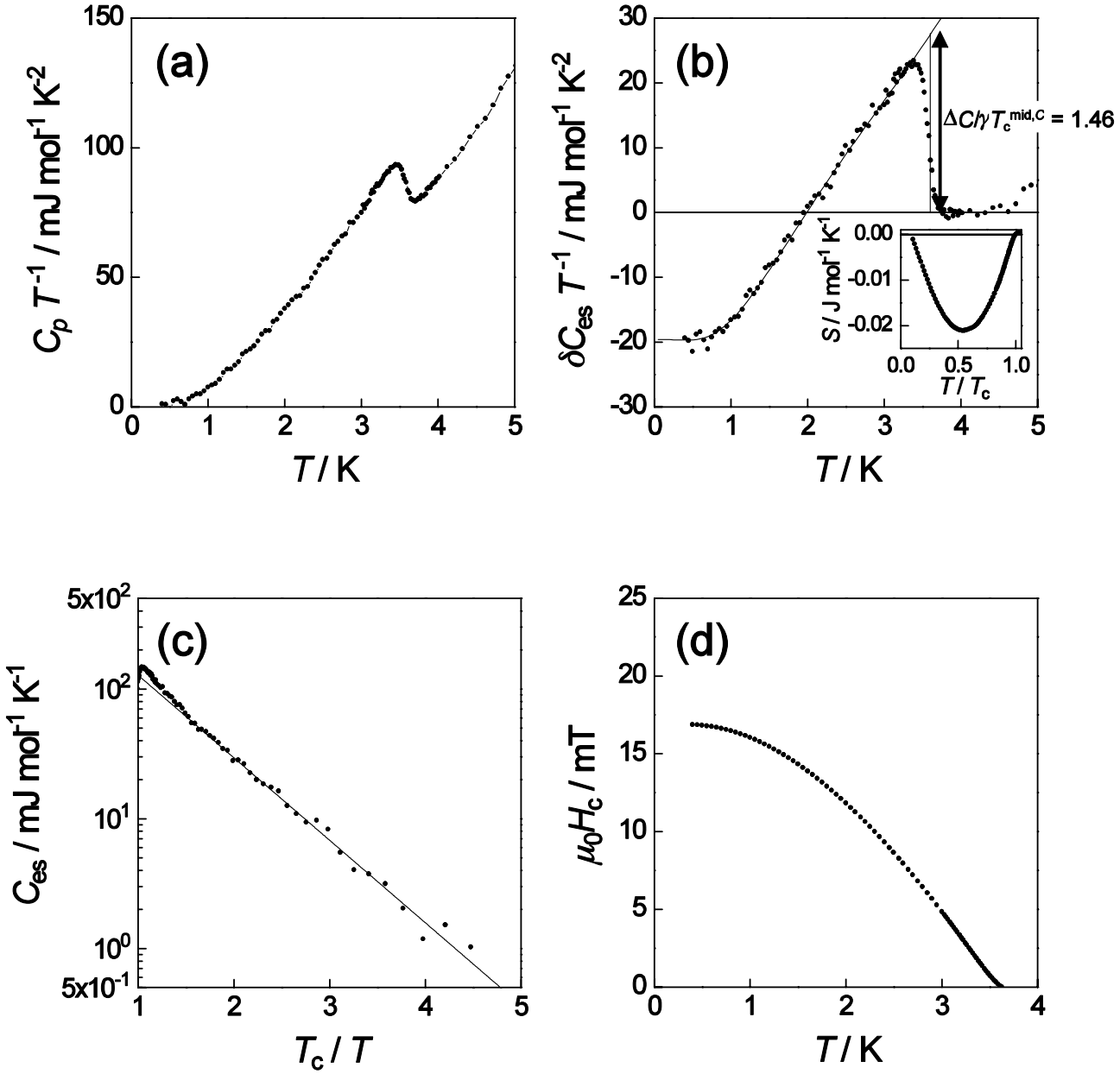
(a)
$C_p\,T^{-1}$ / mJ mol^{-1} K^{-2}
T / K
(b)
$\delta C_{es}\,T^{-1}$ / mJ mol^{-1} K^{-2}
$\Delta C/\gamma T_c^{mid,C}$ = 1.46
S / J mol^{-1} K^{-1}
T / T_c
T / K
(c)
C_{es} / mJ mol^{-1} K^{-1}
T_c / T
(d)
$\mu_0 H_c$ / mT
T / K

Fig.7